Supplementary Materials for

Bacterial turbulence at fluid interfaces

Yuanfeng Yin[1], Bokai Zhang[2*], Shuo Guo[1*]

*Corresponding authors. Email: zbk329@swu.edu.cn, guoshuo@shanghaitech.edu.cn

Vorticity

Distributions of vortex size. In 2D nematic dynamic simulations, the exponential distribution of vortex areas is proposed by L. Giomi (*56*). The density distribution of vortex areas between a_{min} and a_{max} follows:

$$P(a) = \frac{N_\omega}{Z} exp(-a/a*) \tag{S1}$$

where $N_\omega = \int_{a_{min}}^{a_{max}} daP(a)$ is the number of vortices, the normalization factor is given by $Z = \int_{a_{min}}^{a_{max}} dae^{-a/a*}$. In 3D confined bacterial suspensions, this distribution has been widely validated through various experiments (*45*). As shown in Fig. S1, our experiments measure the distributions of vortex areas at the air-liquid surface of the bacterial monolayer, indicating that the exponential form is universal for various fluid thicknesses and bacterial lengths.

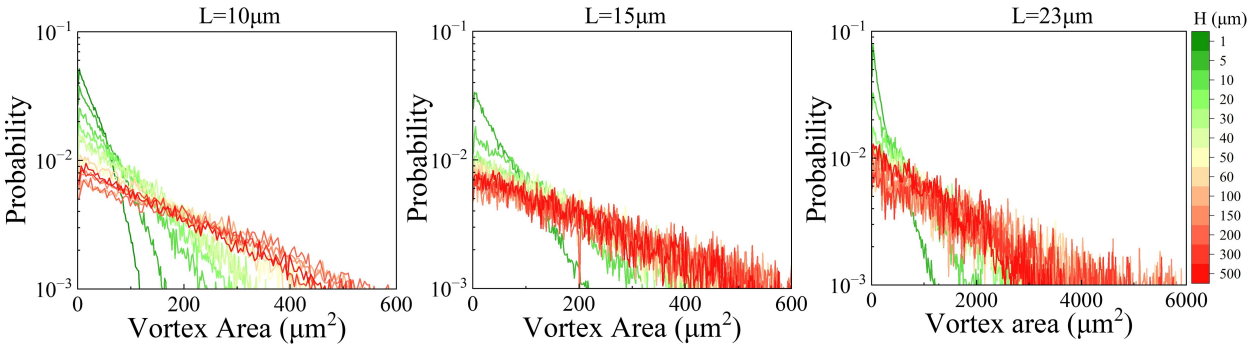

Figure S1: **Exponential distribution of vortez areas.** Density probability distribution of vortex areas for three bacterial lengths at various fluid thicknesses.

Mean-field theory for vorticity power spectrum

In the section, we present the expression for the vortex spectrum in the k-space by closely following Giomi's derivation. The mean-field theory was initially developed for self-similar coherent

structures in two-dimensional decaying turbulence and later extended by Giomi to describe active turbulence. First, the total vorticity at a given position results from the superposition of small vortices, each with a radius R_i, $\omega(\mathbf{r}) = \sum_i \omega_i$. In mean-field theory, the vorticity of the i-th vortex is proposed as a simple distribution, $\omega_i(r) = \omega_{v,i} f_0(r/R_i)$, where $\omega_{v,i}$ is a constant, and r is the distance from the vortex center. The function $f_0(x)$ is defined as $f_0(x) = 0$ for $x > 1$ and $f_0(x) = 1$ for $x \leq 1$, representing a circular unit disk. Therefore, the total vorticity yields

$$\omega(\mathbf{r}) = \sum_i \omega_{v,i} f_0\Big(\frac{\mathbf{r} - \mathbf{r}_i}{R_i}\Big) \tag{S2}$$

The k-space vorticity is obtained by Fourier transform, $\hat{\omega}(\mathbf{k}) = \int \omega(\mathbf{r}) exp(-i\mathbf{k}\cdot\mathbf{r}) d\mathbf{r}$. The function f_0 in k-space is given by:

$$\hat{f_0}(k) = \int d^2 r e^{-i\mathbf{k}\cdot\mathbf{r}} f_0\Big(\frac{r}{R}\Big) = 2\pi \int_0^\infty dr r f_0\Big(\frac{r}{R}\Big) J_0(kr) = 2\pi \int_0^R dr r J_0(kr) = \frac{2\pi R}{k} J_1(kR) \tag{S3}$$

where $k = |\mathbf{k}|$, J_0 and J_1 are Bessel functions of the first kind of order zero and one, respectively. Thus, the k-space vorticity becomes:

$$\hat{\omega}(k) = 2\pi \sum_i \omega_{v,i} \frac{R_i}{k} J_1(kR_i) e^{-i\mathbf{k}\cdot\mathbf{r}_i} \tag{S4}$$

The power spectrum of the vorticity is defined as $|\hat{\omega}(k)|^2$:

$$|\hat{\omega}(k)|^2 = 4\pi^2 \sum_{i,j} \omega_{v,i}\omega_{v,j} e^{-i\mathbf{k}\cdot(\mathbf{r}_i - \mathbf{r}_j)} \frac{R_i R_j}{k^2} J_1(kR_i) J_1(kR_j) \tag{S5}$$

Assuming that spatial correlations between vortices are negligible, only diagonal term are considered,

$$\langle |\hat{\omega}(k)|^2 \rangle = 4\pi^2 \sum_i \omega_{v,i}^2 \frac{R_i^2}{k^2} J_1^2(kR_i) \approx 4\pi^2 \int_{a_{min}}^{a_{max}} dR P_\omega(R) \omega_v^2(R) \frac{R^2}{k^2} J_1^2(kR) \tag{S6}$$

The distribution function of vortex size is related to the distribution of vortex areas: $P_\omega(R) = P_\omega(a)|da/dR|$, where $a = \pi R^2$. Substituting this, we have:

$$\begin{aligned}
\langle |\hat{\omega}(k)|^2 \rangle &= 4\pi^2 \omega_v^2 \int dR P_\omega(a) \Big|\frac{da}{dR}\Big| \frac{R^2}{k^2} J_1^2(kR) \\
&= 8\pi^3 \omega_v^2 \frac{N}{Z} \int dR e^{-a/a^*} \frac{R^3}{k^2} J_1^2(kR) \\
&= (2\pi)^3 \frac{N\omega_v^2}{Z} \frac{1}{k^6} \int d\xi e^{-\xi^2/\kappa^2} \xi^3 J_1^2(\xi) \\
&= \frac{2\pi^3 N \omega_v^2 R^{*6}}{Z} e^{-k^2 R^{*2}/2} \Big[I_0\Big(\frac{k^2 R^{*2}}{2}\Big) - I_1\Big(\frac{k^2 R^{*2}}{2}\Big) \Big]
\end{aligned} \tag{S7}$$

where $\xi = kR$ and $\kappa = kR^*$. The functions I_0 and I_1 represent the modified Bessel functions of the zeroth and first kind, respectively.

Vorticity power spectrum and active force

In a bacterial film, active forces act as a source of vorticity. Based on the Stoke equation without external fluid interactions, the relationship between vorticity and active force in an isolated bacterial film has been established by B. Martinez-Prat *et al.* (*16*) First, the force-balance condition leads to the following Stokes equation,

$$\eta_n \nabla^2 \mathbf{v} - \nabla P + \mathbf{F} = 0 \tag{S8}$$

where η_n is the 2D shear viscosity of the film, and $\mathbf{F}$ is the force density arising from bacterial swimming. Here, we consider an isolated bacterial film, and $\mathbf{F}$ is assumed to be independent of the flow field. Taking the curl of the above equation yields a Poisson equation for the vorticity field $\omega = \hat{\mathbf{z}} \cdot (\nabla \times \mathbf{v})$,

$$\eta_n \nabla^2 \omega = s(\mathbf{r}, t) \tag{S9}$$

where $s(\mathbf{r}, t)$ is the vorticity source due to nematic forces, defined as $s = -\hat{\mathbf{z}} \cdot (\nabla \times \mathbf{F})$. In k-space, the equation becomes

$$-k^2 \hat{\omega}(\mathbf{k}) = \frac{i}{\eta_n}(k_y \hat{F}_x - k_x \hat{F}_y) \tag{S10}$$

Thus, the vorticity spectrum of the active film is related to the source force spectrum as follows:

$$\langle |\hat{\omega}(\mathbf{k})|^2 \rangle = \frac{1}{\eta^2 k^4} \langle k_y^2 |\hat{F}_x|^2 + k_x^2 |\hat{F}_y|^2 - k_x k_y (\hat{F}_x \hat{F}_y^* + \hat{F}_y \hat{F}_x^*) \rangle \tag{S11}$$

Kinetic Energy Spectrum and asymptotic behaviors

In the section, our goal is to establish a simplified theoretical framework to understand the scaling behavior of the energy spectrum at various length scales observed in our experiments. In bacterial flows, the kinetic energy spectrum is determined by both the correlation of active force and the propagator of flow field, and it can be derived using standard procedures (*16, 45*). The active force is associated with the vorticity spectrum, while the propagator depends on the geometry and the boundary conditions of the liquid film. The k-space propagator in the film can be determined using the image reflection method (*49*). The vorticity spectrum is derived from mean-field active liquid

crystal theory in previous section. The asymptotic behaviors and scaling analysis at the long and short wavelengths can be done and is consistent with our experimental measurements.

The kinetic energy per unit mass density, E, in the 2D bacterial suspension is defined as:

$$E = \frac{1}{2}\int \mathbf{v}(\mathbf{R})^2 d^2\mathbf{R} \tag{S12}$$

where $\mathbf{R} \in \{x, y\}$ is the 2D position vector at the air-water interface. Using the 2D Fourier transform, $\hat{F}(\mathbf{k}) = \int F(\mathbf{R}) e^{-i\mathbf{k}\cdot\mathbf{R}} d^2\mathbf{R}$, the angle-averaged kinetic energy is expressed as

$$\langle \hat{E}(k) \rangle = \frac{1}{4\pi S} k \langle |\hat{v}(\mathbf{k})|^2 \rangle \tag{S13}$$

The velocity in k-space is related to the point force generated by bacterial layer through the k-space Green's function $\hat{v}_\alpha = \hat{\mathcal{G}}_{\alpha\beta}\hat{F}_\beta$. Consequently, the angle-averaged kinetic energy is given by:

$$\langle \hat{E}(k) \rangle = \frac{1}{4\pi S} k \hat{\mathcal{G}}_{\alpha\beta}\hat{\mathcal{G}}_{\alpha\gamma} \langle \hat{F}_\beta(\mathbf{k}) \hat{F}_\gamma(\mathbf{k}) \rangle \tag{S14}$$

Here, we present the Green's function in the k space and the force-force correlation function in the liquid film between the air-liquid interface and the solid boundary, as shown in Fig. S2a. The propagating Green's function reflected from the bottom solid plane was modified using the image system derived from Blake's seminar work (*62*). The induced flow field is a combination of

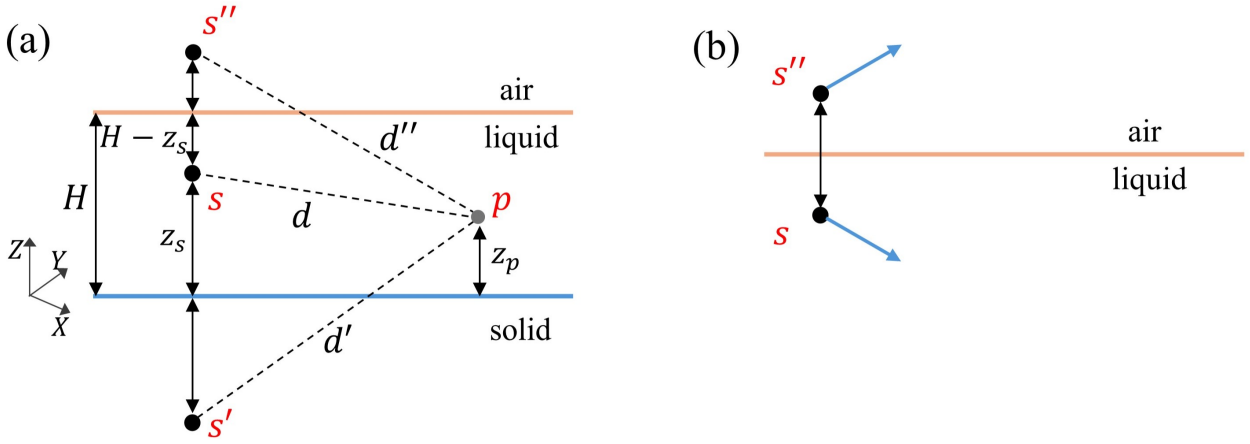

Figure S2: **Schematic diagram of film with perfect-slip air-liquid surface and no-slip solid plane.** The velocity at p generated by Stokeslet s and its two images (s'' and s'). (b) The air-liquid interface induces an image of Stokeslet. The two point forces possess identical components in the xy plane and opposite components along the z-axis.

a Stokeslet and a Stokes doublet, expressed as:

$$\mathcal{G}_{ij}^{plane} = \frac{1}{8\pi}\left\{ -\frac{\delta_{ij}}{d'} - \frac{d'_i d'_j}{d'^3} + 2z\Big(\delta_{j\mu}\delta_{\mu\nu} - \delta_{jz}\delta_{z\nu}\Big)\frac{\partial}{\partial d'_\nu}\left[\frac{z d'_i}{d'^3} - \frac{\delta_{iz}}{d'} - \frac{d'_i d'_z}{d'^3}\right]\right\} \tag{S15}$$

As shown in Fig. S2b, The air-liquid surface at the top is a perfect-slip surface. The fundamental solution induced by this surface is a Stokeslet, given by $\mathcal{G}^{air}(\mathbf{r}) = \mathbf{M}\cdot\mathcal{G}_0(\mathbf{r})$, where $\mathcal{G}_0$ is the Oseen-Burger tensor, $\mathcal{G}_0 = \frac{1}{8\pi\mu}\left(\frac{\delta_{ij}}{r} + \frac{r_i r_j}{r^3}\right)$, and the reflection tensor is $\mathbf{M} = diag(1, 1, -1)$ (*49*).

The horizontal components of the force at point s and its image at s'' are equal, while the normal components of the force exhibit opposite directions. When a force is applied in close proximity to the plane, the normal component of the force and its corresponding image force combine to form a dipole.

Finally, the total Green's function in the liquid film is given by:

$$\begin{aligned}\mathcal{G}_{ij} &= \mathcal{G}_{ij}^{0} + \mathcal{G}_{ij}^{air} + \mathcal{G}_{ij}^{plane} \\ &= \frac{1}{8\pi\mu}\left\{\frac{\delta_{ij}}{d} + \frac{d_i d_j}{d^3} - \frac{\delta_{ij}}{d'} - \frac{d'_i d'_j}{d'^3} + M_{ik}\left(\frac{\delta_{kj}}{d''} + \frac{d''_k d''_j}{d''^3}\right)\right. \\ &\left. + 2z\Big(\delta_{j\mu}\delta_{\mu\nu} - \delta_{jz}\delta_{z\nu}\Big)\frac{\partial}{\partial d'_\nu}\left[\frac{z d'_i}{d'^3} - \frac{\delta_{iz}}{d'} - \frac{d'_i d'_z}{d'^3}\right]\right\}\end{aligned} \tag{S16}$$

The 2D component of the 3D tensor in the xy-plane can be simplified as:

$$\mathcal{G}_{\alpha\beta} = \frac{1}{8\pi\mu}\Big\{ \underbrace{\frac{\delta_{\alpha\beta}}{d} + \frac{d_\alpha d_\beta}{d^3}}_{\langle 1\rangle} - \underbrace{\left(\frac{\delta_{\alpha\beta}}{d'} + \frac{d'_\alpha d'_\beta}{d^3}\right)}_{\langle 2\rangle} + \underbrace{\left(\frac{\delta_{\alpha\beta}}{d''} + \frac{d''_\alpha d''_\beta}{d''^3}\right)}_{\langle 3\rangle} + \underbrace{2zz'\frac{\partial^2}{\partial d'_\alpha \partial d'_\beta}\frac{1}{d'}}_{\langle 4\rangle}\Big\} \tag{S17}$$

where $\alpha, \beta \in \{x, y\}$. The Green's functions in k-space can be derived via a two-dimensional Fourier

transform as outlined in (*50*). For the individual components in eq S17:

$$
\begin{aligned}
\langle 1\rangle &= \frac{1}{\pi^2}\int d^2\mathbf{k}dk_z e^{i\mathbf{k}(\mathbf{R}_p-\mathbf{R}_s)}e^{ik_z(z_p-z_s)}\left[\frac{\delta_{\alpha\beta}}{k^2+k_z^2}-\frac{k_\alpha k_\beta}{(k^2+k_z^2)^2}\right] \\
&= \frac{1}{\pi}\int d^2\mathbf{k}e^{i\mathbf{k}(\mathbf{R}_p-\mathbf{R}_s)}\left[\frac{\delta_{\alpha\beta}}{k}e^{-k|z_p-z_s|}-k_\alpha k_\beta\frac{|z_p-z_s|k+1}{2k^3}e^{-k|z_p-z_s|}\right] \\
\langle 2\rangle &= \frac{1}{\pi}\int d^2\mathbf{k}e^{i\mathbf{k}(\mathbf{R}_p-\mathbf{R}_s)}\left[\frac{\delta_{\alpha\beta}}{k}e^{-k(z_p+z_s)}-k_\alpha k_\beta\frac{(z_p+z_s)k+1}{2k^3}e^{-k(z_p+z_s)}\right] \\
\langle 3\rangle &= \frac{1}{\pi}\int d^2\mathbf{k}e^{i\mathbf{k}(\mathbf{R}_p-\mathbf{R}_s)}\left[\frac{\delta_{\alpha\beta}}{k}e^{-k(2H-z_p-z_s)}-k_\alpha k_\beta\frac{(2H-z_p-z_s)k+1}{2k^3}e^{-k(2H-z_p-z_s)}\right] \\
\langle 4\rangle &= -2z_pz_s\int d^2\mathbf{k}dk_z k_\alpha k_\beta e^{i\mathbf{k}(\mathbf{R}_p-\mathbf{R}_s)}e^{ik_z(z_p+z_s)}\frac{4\pi}{k^2+k_z^2} \\
&= -\frac{z_pz_s}{\pi}\int d^2\mathbf{k}k_\alpha k_\beta e^{i\mathbf{k}(\mathbf{R}_p-\mathbf{R}_s)}\frac{e^{-k(z_p+z_s)}}{k}
\end{aligned}
\tag{S18}
$$

where $\mathbf{k}=\{k_x,k_y\}$ is a 2D vector in the xy-plane, and $k=|\mathbf{k}|$ is the magnitude of the wavevector. $\mathbf{R}_p$ and $\mathbf{R}_s$ are the xy-components of the positions of the velocity point p and force point s, respectively. Using the 2D Fourier tranform,

$$
F(\mathbf{R})=\frac{1}{(2\pi)^2}\int \hat{F}(\mathbf{k})e^{i\mathbf{k}\cdot\mathbf{R}}d^2\mathbf{k} \tag{S19}
$$

the k-space Green's function is readily extracted.

For hydrophobic bacteria swimming in the liquid film, the force point (z_s) and the velocity point (z_p) are located at the air-water interface, with $z_s=z_p=H$. Thus, the total k-space Green's function becomes:

$$
\hat{\mathcal{G}}_{\alpha\beta}=\frac{1}{2\mu}\left\{\left(\frac{\delta_{\alpha\beta}}{k}-\frac{k_\alpha k_\beta}{2k^3}\right)(2+e^{-2kH})-\frac{k_\alpha k_\beta}{2k}\left(\frac{2H}{k}e^{-2kH}-2H^2e^{-2kH}\right)\right\} \tag{S20}
$$

Substituting this into the mean kinetic energy spectrum eq. S14, we have:

$$
\begin{aligned}
\langle E(\mathbf{k})\rangle &= \frac{1}{4\pi A}k\hat{\mathcal{G}}_{\alpha\beta}\hat{\mathcal{G}}_{\alpha\gamma}\langle\hat{F}_\beta(k)\hat{F}_\gamma(k)\rangle \\
&= \frac{1}{4\pi A}k\Bigg[\left(\frac{\delta_{\alpha\beta}}{k}-\frac{k_\alpha k_\beta}{2k^3}\right)\left(\frac{\delta_{\alpha\nu}}{k}-\frac{k_\alpha k_\nu}{2k^3}\right)(2+e^{-2kH})^2\langle\hat{F}_\beta\hat{F}_\gamma^*\rangle \\
&- \frac{k_\beta k_\gamma}{4k^2}\langle\hat{F}_\beta\hat{F}_\gamma^*\rangle(2+e^{-2kH})\left(\frac{2H}{k}-2H^2\right)*e^{-2kH}+\frac{k_\beta k_\gamma}{4}\left(\frac{2H}{k}-2H^2\right)^2*e^{-4kH}\langle\hat{F}_\beta\hat{F}_\gamma^*\rangle\Bigg] \\
&= \frac{1}{4\pi A}k\Bigg\{\frac{(2+e^{-2kH})^2}{k^4}\langle k_y^2\hat{F}_x^2+k_x^2\hat{F}_y^2-k_xk_y(\hat{F}_x\hat{F}_y^*+\hat{F}_y\hat{F}_x^*)\rangle \\
&+ \left[\frac{2+e^{-2kH}}{2k}-\frac{k}{2}\left(\frac{2H}{k}-2H^2\right)*e^{-2kH}\right]^2\langle\hat{F}^2\rangle\Bigg\}
\end{aligned}
\tag{S21}
$$

where $\hat{F}^2 = \hat{F}_x^2 + \hat{F}_y^2$. Substituting the vorticity eq. S11 into this result yields:

$$\langle E(\mathbf{k})\rangle = \frac{k}{4\pi S}\left\{\eta_n^2\langle|\hat{\omega}(\mathbf{k})|^2\rangle(2+e^{-2kH})^2 + \left[\frac{2+e^{-2kH}}{2k} - k\left(\frac{H}{k}-H^2\right)e^{-2kH}\right]^2\langle\hat{F}^2\rangle\right\} \tag{S22}$$

The asymptotic behaviors of the kinetic energy spectrum for small and large kH, with respect to vorticity and k, are given by

$$\langle E(\mathbf{k})\rangle \sim \eta_n^2 k\langle|\hat{\omega}(\mathbf{k})|^2\rangle + \frac{\langle\hat{F}^2\rangle}{4k} \tag{S23}$$

Assuming $F \ll \eta\omega k$, the scaling behaviors of the kinetic energy spectrum in 2D interfacial bacterial turbulence is entirely determined by the asymptotic behavior of the vorticity. According to eq. S14, the asymptotic scaling of the vorticity spectrum for small and large kR^* is given as

$$\begin{aligned}\lim_{kR^*\to\infty}\langle|\hat{\omega}(\mathbf{k})|^2\rangle &\sim \frac{1}{(kR^*)^3}\\ \lim_{kR^*\to 0}\langle|\hat{\omega}(\mathbf{k})|^2\rangle &\sim (kR^*)^0\end{aligned} \tag{S24}$$

In experiment, we observe that the vortex size becomes comparable to the liquid height when $H < 100\mu m$. Consequently, our analysis focuses on cases where k is either smaller than both $1/R^*$ and $1/H$, or greater than $1/R^*$ and $1/H$. The asymptotic behavior of the energy spectrum for narrow and large liquid films can then be expressed as:

$$\begin{aligned}\langle E(\mathbf{k})\rangle &\sim k, && \left(k \ll \frac{1}{R^*}, \frac{1}{H}\right)\\ \langle E(\mathbf{k})\rangle &\sim \frac{1}{k^2}, && \left(k \gg \frac{1}{R^*}, \frac{1}{H}\right)\end{aligned} \tag{S25}$$

Hydrodynamic instability

Flow field of the film between the air-liquid interface and the solid plane. In mean-field kinetic theory, we treat the bacteria as dipoles and calculate the flow induced by a force dipole κ with orientation $\mathbf{p}$ located in the liquid film between the air-liquid interface and the solid plane as shown in Fig. S2. The velocities are obtained through the first two images reflected by the boundaries:

$$\begin{aligned}\mathbf{u}^{s} &= \frac{\kappa}{8\pi}\frac{\mathbf{x}}{d^3}\left[\frac{3(\mathbf{x}\cdot\mathbf{p})^2}{d^2} - 1\right]\\ \mathbf{u}^{s'} &= \frac{\kappa}{8\pi}\left[\frac{\mathbf{x}'}{d'^3} - \frac{3\mathbf{x}'(\mathbf{x}'\cdot\mathbf{p})^2 + 6h^2(\mathbf{x}' + 2\mathbf{p}(\mathbf{x}'\cdot\mathbf{p}))}{d'^5} + \frac{30h^2(\mathbf{x}'\cdot\mathbf{p})^2\mathbf{x}'}{d'^7}\right]\\ \mathbf{u}^{s''} &= \frac{\kappa}{8\pi}\frac{\mathbf{x}''}{d''^3}\left[\frac{3(\mathbf{x}''\cdot\mathbf{p})^2}{d''^2} - 1\right]\end{aligned} \tag{S26}$$

where $\mathbf{u}^s$ is the flow field in an unbounded geometry, $\mathbf{u}^{s'}$ is the velocity induced by the no-slip boundary at the bottom, and $\mathbf{u}^{s'}$ is the velocity induced by the air-liquid interface. The orientation is taken as $\mathbf{p} = \{p_x, p_y\}$. The flow field in k-space is obtained using the 2D Fourier transform, defined as $\hat{u}_\alpha(\mathbf{k}, \mathbf{p}) = \int d^2\mathbf{x} u_\alpha(\mathbf{x}, \mathbf{p}) exp(-i\mathbf{k} \cdot \mathbf{x})$. These velocities are given by

$$\begin{aligned}
\hat{u}_\alpha^{s,s''} &= \frac{\kappa}{8\pi} \int \frac{x_\alpha}{(r^2+z^2)^{3/2}} \Big[\frac{3(x_\beta p_\beta)^2}{r^2+z^2} - 1 \Big] e^{-i\mathbf{k}\cdot\mathbf{x}} d^2x \\
&= -\frac{i\kappa}{8\pi} \frac{\partial}{\partial k_\alpha} \int \Big[\frac{1}{(r^2+z^2)^{3/2}} + \frac{\partial^2}{\partial k_x^2} \frac{3p_x^2}{(r^2+z^2)^{5/2}} + \frac{\partial^2}{\partial k_y^2} \frac{3p_y^2}{(r^2+z^2)^{5/2}} + \frac{\partial^2}{\partial k_x k_y} \frac{6p_x p_y}{(r^2+z^2)^{5/2}} \Big] e^{-i\mathbf{k}\cdot\mathbf{x}} d^2x
\end{aligned} \tag{S27}$$

$$\begin{aligned}
\hat{u}_\alpha^{s'} &= \frac{\kappa}{8\pi} \int \Big[\frac{x'_\alpha}{(r^2+z^2)^{3/2}} - \frac{3x'_\alpha (x'_\beta p_\beta)^2 + 6h^2(x'_\alpha + 2p_\alpha(x'_\beta p_\beta))}{(r^2+z^2)^{5/2}} + \frac{30h^2 x'_\alpha (x'_\beta p_\beta)^2}{(r^2+z^2)^{7/2}} \Big] e^{-i\mathbf{k}\cdot\mathbf{x}} d^2x \\
&= \frac{i\kappa}{8\pi} \frac{\partial}{\partial k_\alpha} \int \Big\{ \frac{1}{(r^2+z^2)^{3/2}} + \frac{6h^2}{(r^2+z^2)^{5/2}} - \frac{\partial^2}{\partial k_x^2} \frac{3p_x^2}{(r^2+z^2)^{5/2}} - \frac{\partial^2}{\partial k_x k_y} \frac{6p_x p_y}{(r^2+z^2)^{5/2}} - \frac{\partial^2}{\partial k_y^2} \frac{3p_y^2}{(r^2+z^2)^{5/2}} \\
&- 30h^2 \Big[\frac{\partial^2}{\partial k_x^2} \frac{p_x^2}{(r^2+z^2)^{7/2}} - \frac{\partial^2}{\partial k_y^2} \frac{p_y^2}{(r^2+z^2)^{7/2}} - \frac{\partial^2}{\partial k_x k_y} \frac{2p_x p_y}{(r^2+z^2)^{7/2}} \Big] \Big\} e^{-i\mathbf{k}\cdot\mathbf{x}} d^2x \\
&+ \frac{i\kappa}{8\pi} \frac{\partial}{\partial k_\beta} \int \frac{12h^2 p_\beta p_\alpha}{(r^2+z^2)^{5/2}} e^{-i\mathbf{k}\cdot\mathbf{x}} d^2x
\end{aligned} \tag{S28}$$

where r is the distance between velocity and force points at xy-plane. For points s, s', and s'', r is the same. The height difference, z, is defined as $z = |z_s - z_p|$ for the dipole in the film, $z = z_s + z_p$ for the image from the non-slip boundary, and $z = 2H - z_s - z_p$ for the image reflected by the air-liquid interface. In the work, we measure the vortex and energy spectrum at the air-liquid interface. Therefore, z_s and z_p are taken as H.

Derivation for growth rate equation. By substituting the velocity spectra derived in the preceding section into eq. 9 and 10, it is observed that the integral depends solely on the angle between the dipole orientation vector and the wave vector. For simplicity, the direction of the wave vector $\mathbf{k}$ can be aligned with the x-axis. Upon integration, eq. 9 and 10 yield an eigenvalue problem as follows:

$$\begin{bmatrix} M_{11} - 1 & 0 & 0 \\ M_{21} & M_{22} - 1 & ikM_{23} \\ 0 & ikM_{32} & M_{33} - 1 \end{bmatrix} \cdot \begin{bmatrix} \delta\hat{U}_\perp \\ \delta\hat{U}_\parallel \\ \delta\hat{\rho} \end{bmatrix} = 0 \tag{S29}$$

where $\delta\hat{U}_\parallel$ is the longitudinal velocity perturbation along k direction, and $\delta\hat{U}_\perp$ is the transverse

velocity perturbation normal to k-direction. The matrix elements are listed as follows:

$$
\begin{aligned}
M_{11} &= \frac{nB\kappa}{v_s}\frac{2+b^2-2\sqrt{1+b^2}}{2b^3}[2-(1-kH)e^{-2kH}] \\
M_{21} &= -\frac{nB\kappa}{v_s}kHe^{-kH}\frac{2+b^2-2\sqrt{1+b^2}}{b^3} \\
M_{23} &= \frac{\kappa\lambda}{v_sk^2}\frac{1}{2b}\Big(\frac{1}{\sqrt{1+b^2}}-1\Big)-\frac{\kappa\lambda}{v_sk^2}\frac{1}{4b}\Big(\frac{1}{\sqrt{1+b^2}}-1\Big)(1-Hk+2H^2k^2)e^{-kH} \\
M_{32} &= \frac{n}{v_sk}\frac{2B(\sqrt{1+b^2}-1)-b^2(1+B)}{b\sqrt{1+b^2}} \\
M_{33} &= \frac{\lambda}{v_sk}\frac{b}{\sqrt{1+b^2}} \\
M_{22} &= \frac{n\kappa}{v_s}\frac{(b^2(\sqrt{1+b^2}-1-B)+2B(\sqrt{1+b^2}-1))(1-2e^{2kH}-2kH+2k^2H^2)e^{-2kH}}{4b^3\sqrt{1+b^2}}
\end{aligned}
\tag{S30}
$$

where $b = v_sk/(\chi+\lambda)$. The presence of air-liquid interface introduces a non-diagonal term, M_{21}, but since $M_{12} = 0$, the longitudinal mode and density fluctuation do not influence the stability of the transverse mode. We analyses the orientational instability by considering the transverse mode (*36*),

$$
M_{11} = 1 = \frac{nB\kappa}{v_s}\frac{2+b^2-2\sqrt{1+b^2}}{2b^3}[2-(1-kH)e^{-2kH}] \tag{S31}
$$

The equation could be solved analytically as:

$$
b^{-1} = G\Big(\frac{2v_sf(kH)}{B\kappa n}\Big)\frac{B\kappa n}{2v_sf(kH)} \tag{S32}
$$

where $f(x)$ arises from the effect of fluid thickness and is defined as:

$$
f(x) = \frac{1}{2-xe^{-2x}} \tag{S33}
$$

As a result, the growth rate equation χ is derived,

$$
\chi = -\lambda + G\Big(\frac{2v_s}{B\kappa n}\Big)\frac{B\kappa n}{2v_sf(kH)} \tag{S34}
$$

where $G(x) = 6x^2[4-(1\pm i\sqrt{3})/h(x)-(1\mp i\sqrt{3})h(x)]^{-1}$ and $h(x) = [54x^2-1+6\sqrt{3}x\sqrt{27x^2-1}]^{1/3}$. For deterministic swimming ($\lambda = 0$), the orientation instability occurs when $x < 1/\sqrt{2}$, where the real part of the function $G(x)$ becomes positive. Two distinct instability regimes are identified: one without oscillation ($\mathrm{Im}[G] = 0$) and one with oscillation ($\mathrm{Im}[G] \neq 0$), as shown in Fig. S3.

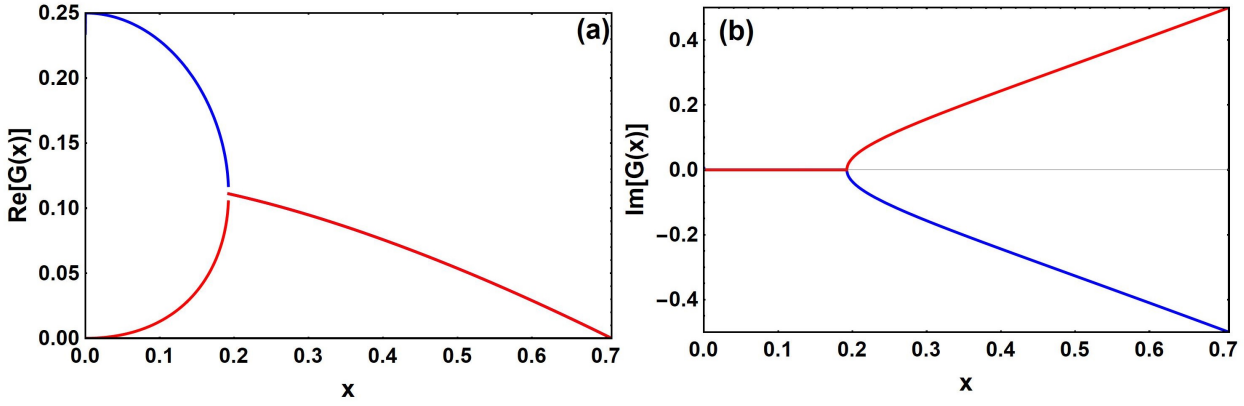

Figure S3: **Instability of growth rate equation.** The real and imaginary parts of the function $G(x)$ for $x < 1/\sqrt{2}$.

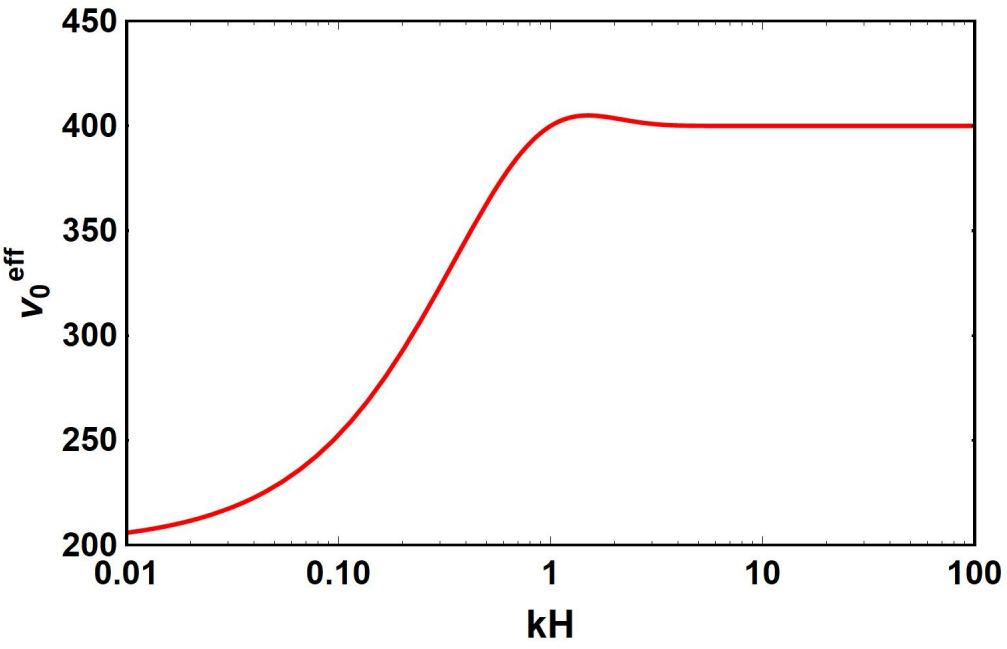

Figure S4: **Dependence of effective intrinsic velocity on liquid thickness.** Effective intrinsic velocity as a function of kH at $v_0 = 200\mu m/s$.

Scaling behaviors between vortex size and fluid thickness

At the onset of instability ($\chi = 0$), the growth rate λ is given by

$$\lambda = G\Big(\frac{2v_s f(kH)}{v_0}\Big)\frac{v_0 k}{2f(kH)} \tag{S35}$$

where $v_0 \equiv B\kappa n$. Using the scaling argument $G(x) \sim x^\gamma$, we obtain, after some algebra,

$$f(kH)^{\gamma-1}k = \frac{2\lambda}{v_0}\Big(\frac{v_0}{2v_s}\Big)^\gamma = C \tag{S36}$$

with C being a constant independent of the wavevector. If $f(x)$ follows the scaling relation $f \sim x^\beta$, we then have

$$k^{\beta(\gamma-1)}H^{\beta(\gamma-1)}k = C \tag{S37}$$

Considering $k = 2\pi/R_v$, the scaling relation between vortex size and fluid thickness is

$$R_v \sim H^{\frac{\beta(1-\gamma)}{\beta-1-\beta\gamma}} \tag{S38}$$

Thus, $R_v \sim H^\alpha$, where the scaling exponent α is determined by two contributions: i) the exponent β, depending on the flow propagation in the film, ii) the exponent γ, associated with bacterial swimming as a dipole in the two-dimensional plane embedded in the three-dimensional fluid. Estimating α for intermediate fluid thicknesses from experimental bacterial parameters ($v_0 = B\kappa n = 200\mu m/s$,$\lambda = 1s^{-1}$), MFKT predicts a critical reduced wavevector $k_c^r \equiv kH \approx 0.29$ at $H = 10\mu m$. As shown in Fig. S5, the corresponding exponents are $\beta = -0.244$ and $\gamma = -0.37$, yielding

$$\alpha = \frac{\beta(1-\gamma)}{\beta-1-\beta\gamma} \approx 0.25 \tag{S39}$$

which is consistent with both our experimental measurements and theoretical predictions.

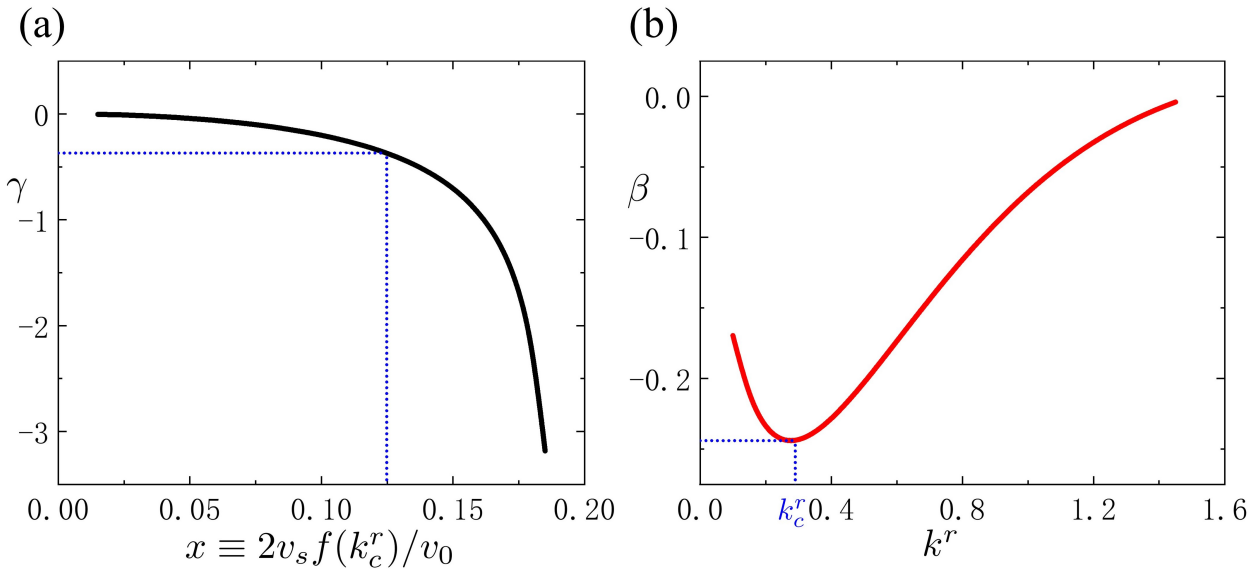

Figure S5: **Scaling exponents of functions** $G(x)$ **and** $f(kH)$ (a) The scaling exponent γ in function G as a function of $x \equiv 2v_s f(k_c)/v_0$. (b) The scaling exponent β in function $f(x)$ as a function of $k^r \equiv kH$. The dashed line indicates the values of these exponents at intermediate thickness $H = 10\mu m$, $v_0 \equiv B\kappa n = 200\mu m/s$, and $\lambda = 1s^{-1}$.

Experimental supplementary figures

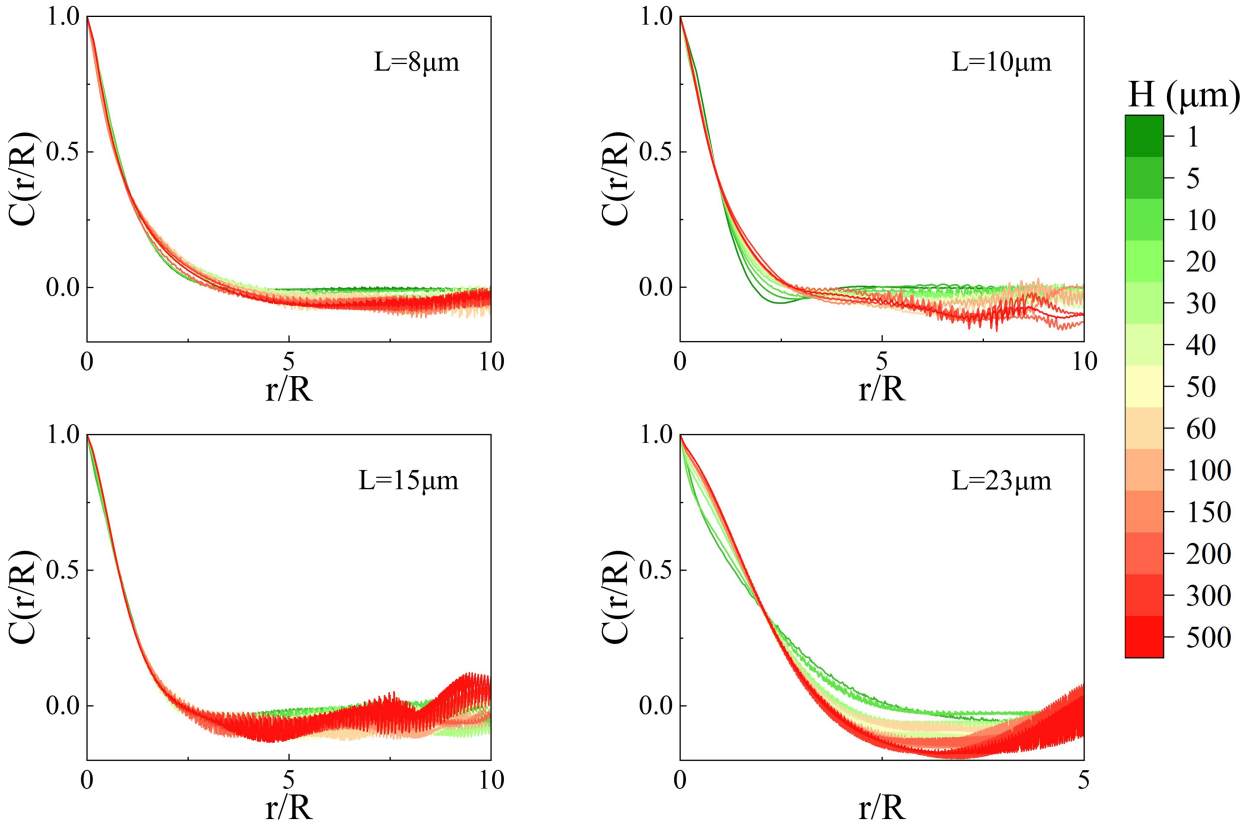

Figure S6: **Velocity correlations.** Velocity correlation functions for varying fluid thicknesses and four bacterial lengths.

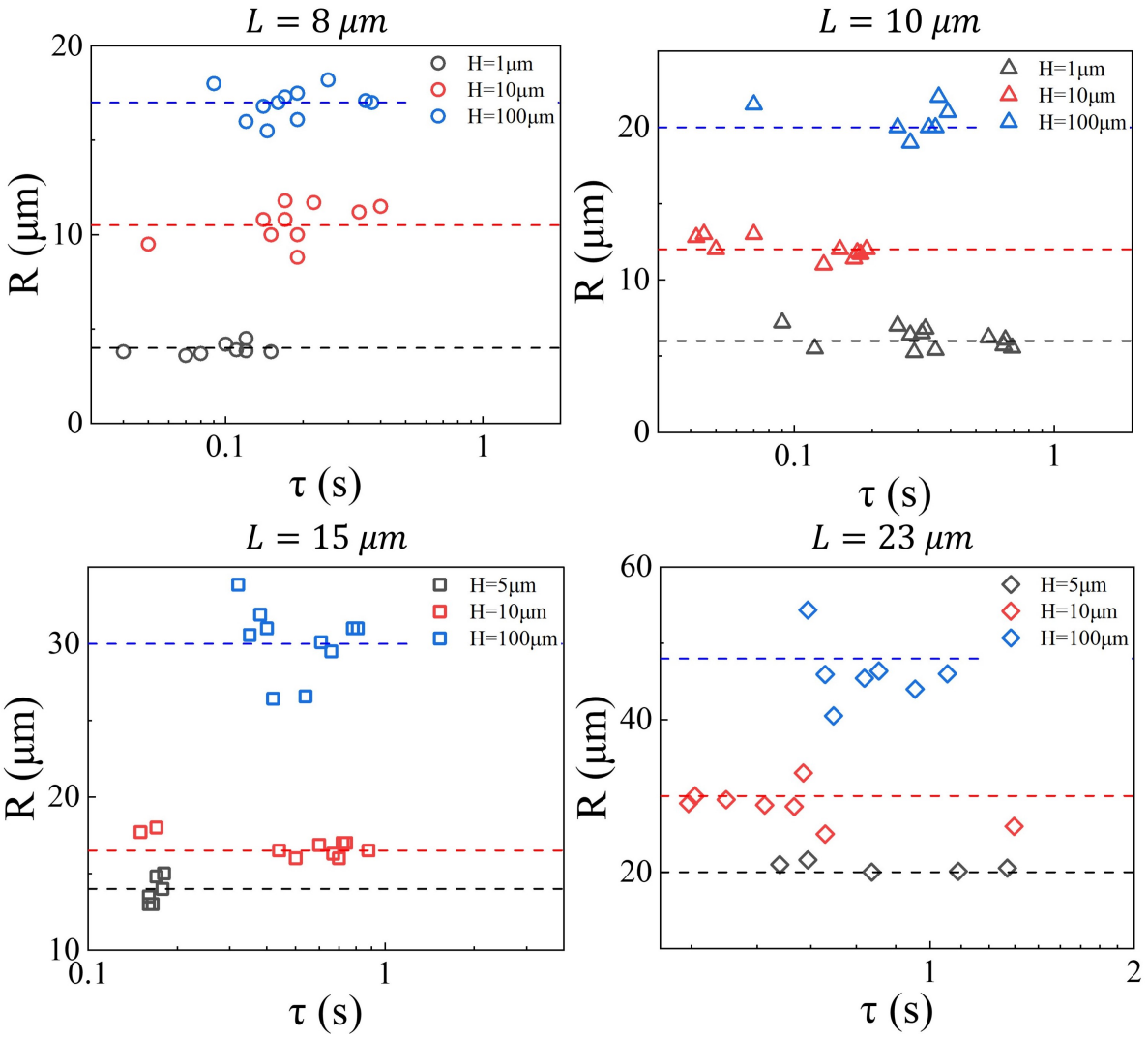

Figure S7: **Correlation lengths.** Correlation lengths as a function of correlation time for three fluid thicknesses and four bacterial lengths.

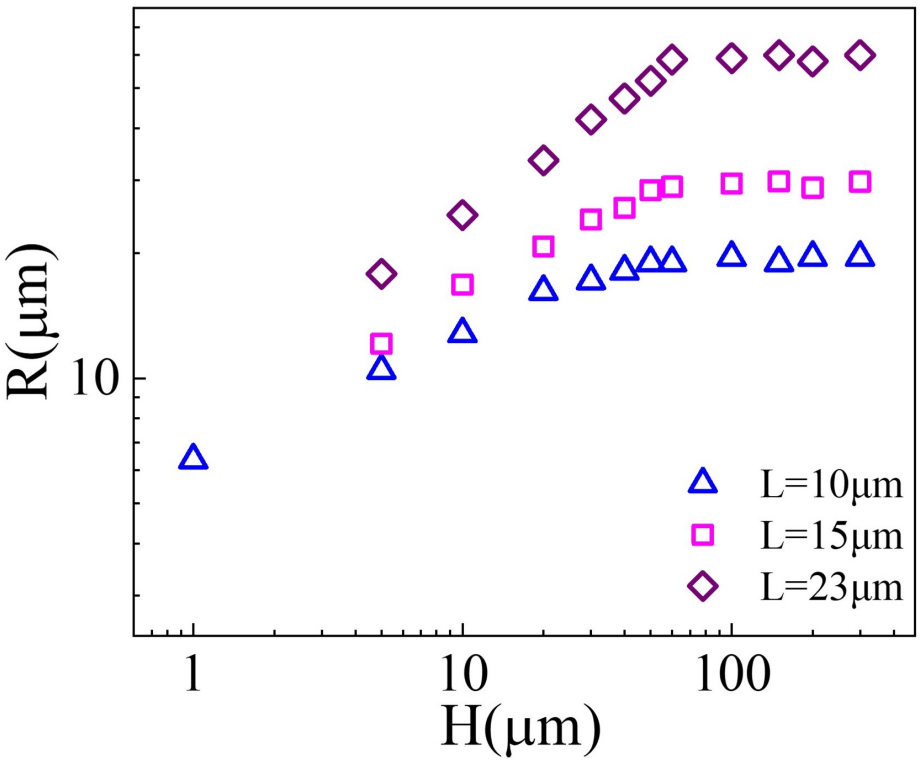

Figure S8: **Dependence of vortex size on liquid thickness.** Vortex size is measured based on the velocity field using an Okubo-Weiss (OW) method.

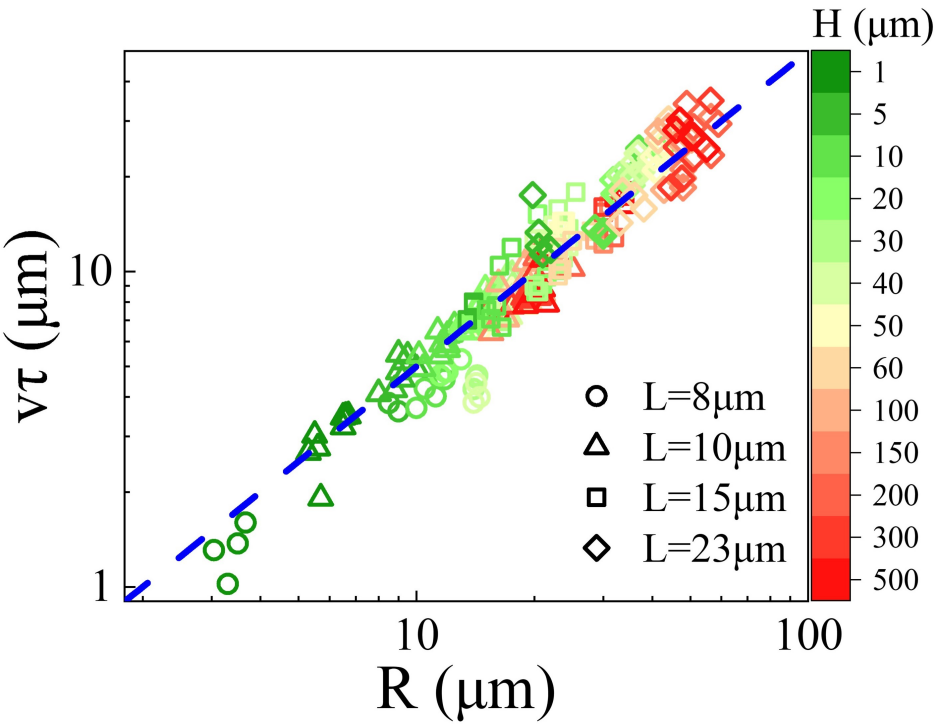

Figure S9: **Relationships between characteristic lengths.** The product of the correlation time and mean fluid speed is proportional to the correlation length.

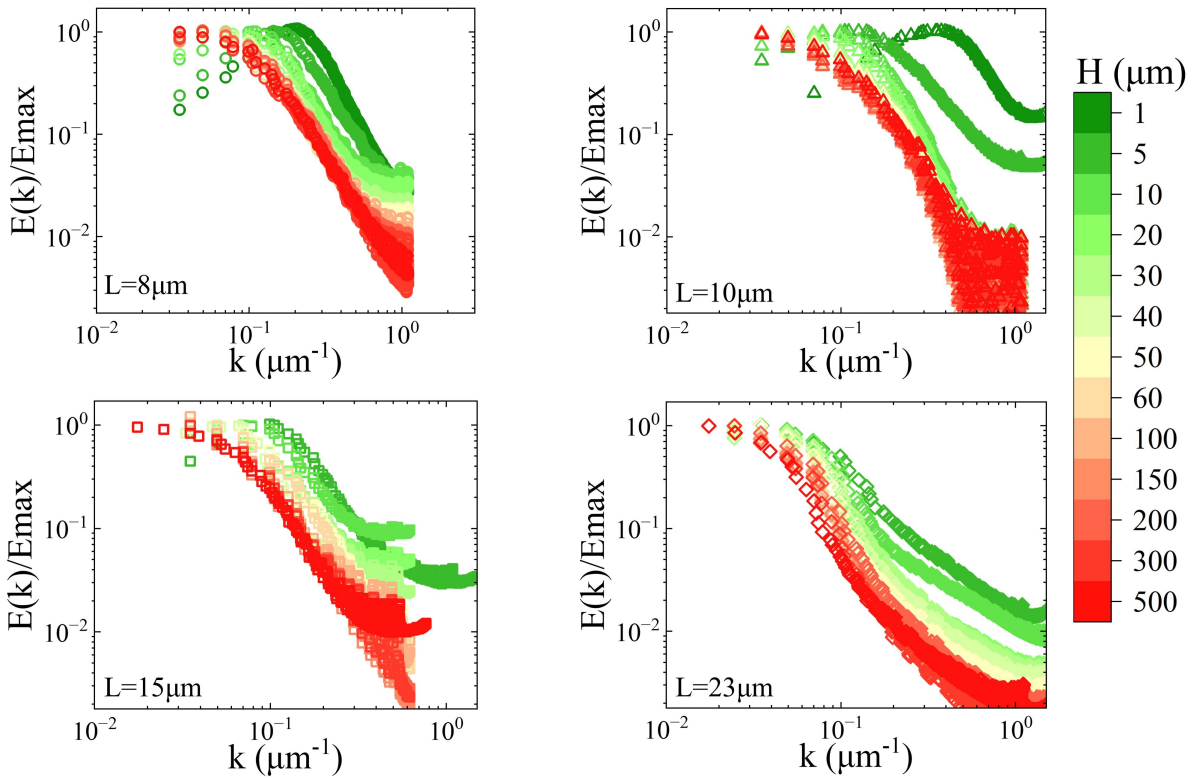

Figure S10: **Direct measurements for kinetic energy spectrum .** Normalized kinetic energy spectrum (relative to the maximum value) for varying fluid thicknesses and four different bacterial lengths.

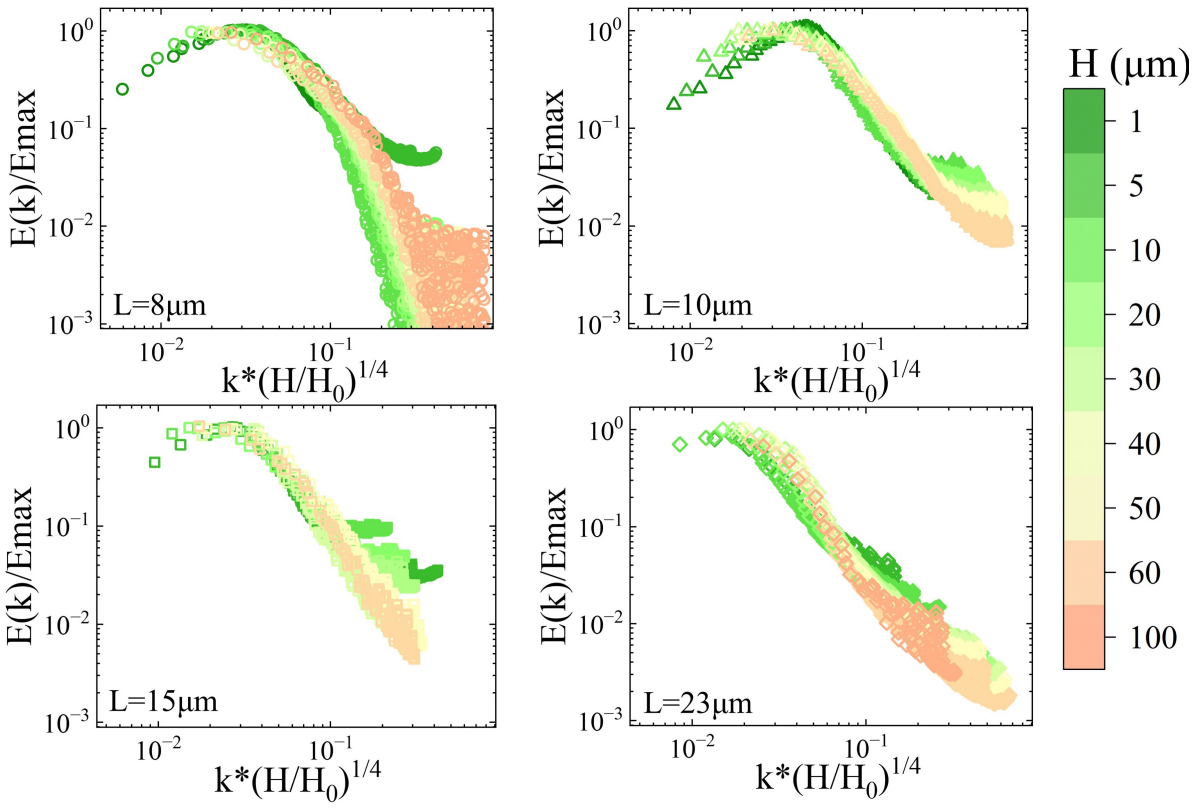

Figure S11: **The collapse of the normalized kinetic energy spectrum.** Normalized kinetic energy spectrum as a function of reduced fluid thickness, multiplied by $(H/H_0)^{1/4}$, where $H_0 = 100\mu m$, for four different bacterial lengths.